SANDIA REPORT

SAND2006-7894
Unlimited Release
Printed December 2006
Revision 1.0

Model-Based Statistical Estimation of Sandia RF Ohmic Switch Dynamic Operation from Stroboscopic, X-ray Imaging

Carl Diegert

Prepared by
Sandia National Laboratories
Albuquerque, New Mexico 87185 and Livermore, California 94550

Sandia is a multiprogram laboratory operated by Sandia Corporation,
a Lockheed Martin Company, for the United States Department of Energy's
National Nuclear Security Administration under Contract DE-AC04-94AL85000.

Issued by Sandia National Laboratories, operated for the United States Department of Energy by Sandia Corporation.

Available to DOE and DOE contractors from
U.S. Department of Energy
Office of Scientific and Technical Information
P.O. Box 62
Oak Ridge, TN 37831
Telephone: (865) 576-8401
Facsimile: (865) 576-5728
E-Mail: reports@adonis.osti.gov
Online ordering: http://www.osti.gov/bridge

Available to the public from
U.S. Department of Commerce
National Technical Information Service
5285 Port Royal Rd.
Springfield, VA 22161
Telephone: (800) 553-6847
Facsimile: (703) 605-6900
E-Mail: orders@ntis.fedworld.gov
Online order: http://www.ntis.gov/help/ordermethods.asp?loc=7-4-0#online

SAND2006-7894
Unlimited Release
Printed December 2006
Revision 1.0

Model-Based Statistical Estimation of Sandia RF Ohmic Switch Dynamic Operation from Stroboscopic, X-ray Imaging

Carl Diegert
Computational Biology Department
Sandia National Laboratories
P.O. Box 5800
Albuquerque, New Mexico 87185-MS0822

Abstract

We define a new diagnostic method where computationally-intensive numerical solutions are used as an integral part of making difficult, non-contact, nanometer-scale measurements. The limited scope of this report comprises most of a due diligence investigation into implementing the new diagnostic for measuring dynamic operation of Sandia's RF Ohmic Switch. Our results are all positive, providing insight into how this switch deforms during normal operation. Future work should contribute important measurements on a variety of operating MEMS devices, with insights that are complimentary to those from measurements made using interferometry and laser Doppler methods. More generally, the work opens up a broad front of possibility where exploiting massive high-performance computers enable new measurements.

CONTENTS

FIGURES

TABLES

INTRODUCTION

We define a new diagnostic method where computationally-intensive numerical solutions are used as an integral part of making difficult, non-contact, nanometer-scale measurements. The limited scope of this report comprises most of a due diligence investigation into implementing the new diagnostic for measuring dynamic operation of Sandia's RF Ohmic Switch.

The new diagnostic is enabled as much by dramatic advances in the predictive capability obtained by applying numerical simulation tools as by evolutionary advances in microscopic imaging using X-rays and light. Numerical simulation and physical measurement are cornerstones of the Science-Based Engineering Transformation initiative, SBET, at Sandia National Laboratories. Sandia's current switch design effort fully embraces the traditional SBET workflow, with numerical simulation experiments applied to evaluate engineering alternatives, thus eliminating the time and expense of fabricating and measuring experimental switch parts. Ultimately Sandia fabricates and measures physical switch parts. If switch performance is acceptable, then the parts are shipped to Sandia's customers. Measurements on physical parts are almost always a basis for iterating the whole SBET process. Iteration can advance modeling and simulation capability, and consequently advance switch performance beyond current customer demands.

The new diagnostic method described in the next section of this report constitutes an innovation in the SBET workflow; the new diagnostic shows how the modeling and numerical simulation that enables the virtual SBET design iterations can also enable new capability in measuring physical parts.

Our results are all positive, providing insight into how this switch deforms during normal operation. Future work should contribute important measurements on a variety of operating MEMS devices, with insights that are complimentary to those from measurements made using interferometry and laser Doppler methods. More generally, the work opens up a broad front of possibility where the ability of massive high-performance computers enables new measurements.

MATERIALS AND METHODS

Understanding how an operating MEMS component deforms can be a key to creating a design that is robust to manufacturing variation, or that exhibits long lifetime. Engineering measurement using general-purpose diffraction or interferometric techniques may be difficult or impossible because resolution is limited or because views are occluded. We propose a measurement methodology that is specialized to measuring deformation of the crab component in the Sandia Ohmic RF Switch MEMS device. The methodology gains enormous statistical power relative to general-purpose imaging techniques by replacing the general problem of measuring an arbitrary device under test with a model-based statistical estimation problem based on a low-degree-of-freedom *summary model* of the device known to be under test. The model-based measurement methodology is a two step process:

First, we define a *summary model*. The summary model is defined so that, with variations in summary model parameter values, all physically-possible deformations of the crab are captured. In constructing the summary model variations in as-fabricated geometry, forces produced during operation, and other conditions are *not* statistically modeled. Instead, we set bounds on these variations so that *all* possible deformations are captured.

Second, we image the physical part using light or X-rays and process the imaging information to estimate summary model parameter values. Computed estimates specify the particular deformation that is most consistent with the high-degree-of-freedom, non-contact imaging measurement. This second part is classical statistical estimation theory.

Statistical estimation based on the summary model can be vastly more powerful than results where images are estimated without knowledge of what is imaged. For measuring deformation of the switch crab, the statistical power gained by basing estimation on a summary model should enable estimation of crab deformation using only an X-ray view of the MEMS component taken perpendicular to the plane of the MEMS substrate. Without the summary model, we would have to resolve movement of only a few nanometers as directly measured in these X-ray images.

Resolving features at this scale, a scale smaller than the wavelength of the X-rays, is beyond the capability of the state-of-the-art imaging X-ray machines.

Defining an effective summary model is a creative process. For a completely-defined set of initial conditions, a finite-element analysis, FEA, of the switch crab gives the resulting deformation of the crab with enough fidelity that we can just assume that the FEA solution is physically correct. A series of FEA solutions can help define a summary model that includes all physically-possible deformations. A large computing resource can help by delivering a wealth of high-fidelity solutions to particular problem instances. Human insight and creativity in discovering bounding arguments is also part of defining the summary model.

To define a summary model for the switch crab, we can usefully assume that the as-fabricated mass of the electro-deposited gold crab will not change during switch operation. Additional assumptions bounding ductile changes in the gold, together with knowledge accumulated from a series of high-fidelity FEA solutions, should be able to characterize all possible deformation motions of the crab during short-term measurements of the operating switch as a superposition of well-defined mode shapes. The parameter values for this mode-shape summary model, then, define the specific shapes, and define the weights in their weighted sum.

RESULTS

The limited scope of this report comprises most of a due diligence investigation into implementing a new diagnostic for measuring dynamic operation of Sandia's RF Ohmic Switch. Table 1 gives the six areas where we have results, and gives our subjective assessment of the risk to success with the new diagnostic from aspects of completing work in that area. The next five parts of this report describe our results.

Table 1. Due diligence investigation results for a new method for measuring dynamic operation of Sandia's RF Ohmic MEMS switch are in the five areas in this table.

Static X-ray imaging Can COTS X-ray machine acquire adequate static images of switch part?	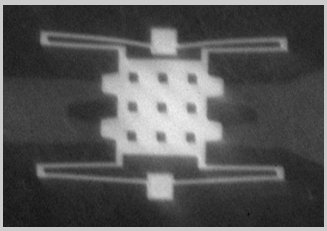
Dynamic X-ray imaging Can COTS X-ray machine acquire adequate dynamic images of switch part?	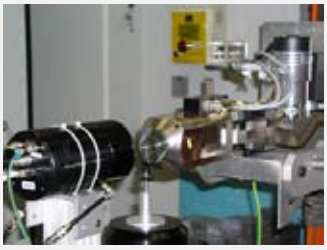
Ground Truth Surface topography Can ultraviolet confocal light microscope provide *ground truth* crab deformation?	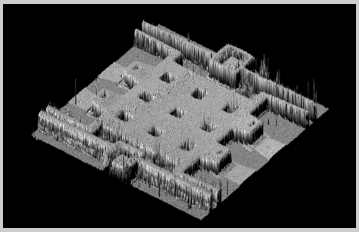
Deformation from MIP light image Can summary-model statistical analysis of Maximum Intensity Projection confocal images (surrogate for X-ray image) predict 3D crab deformation?	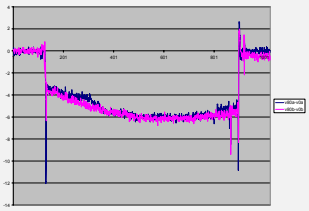
Deformation from X-ray image Can summary-model statistical analysis of X-ray imaging taken perpendicular to switch substrate predict 3D crab deformation?	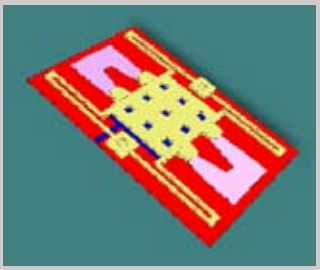

Figure 1 shows a the Sandia Ohmic RF Switch MEMS part placed on the tip of a fluidic fixture from an unrelated MEMS project by Murat Okandan, Sandia National Laboratories organization 01749. The distance from the 6 to the 7 on the scale is 0.1 inches. Ken acquired the image in his ceramics lab. This Sandia MEMS part includes two independent ohmic RF switches on the single alumina substrate.

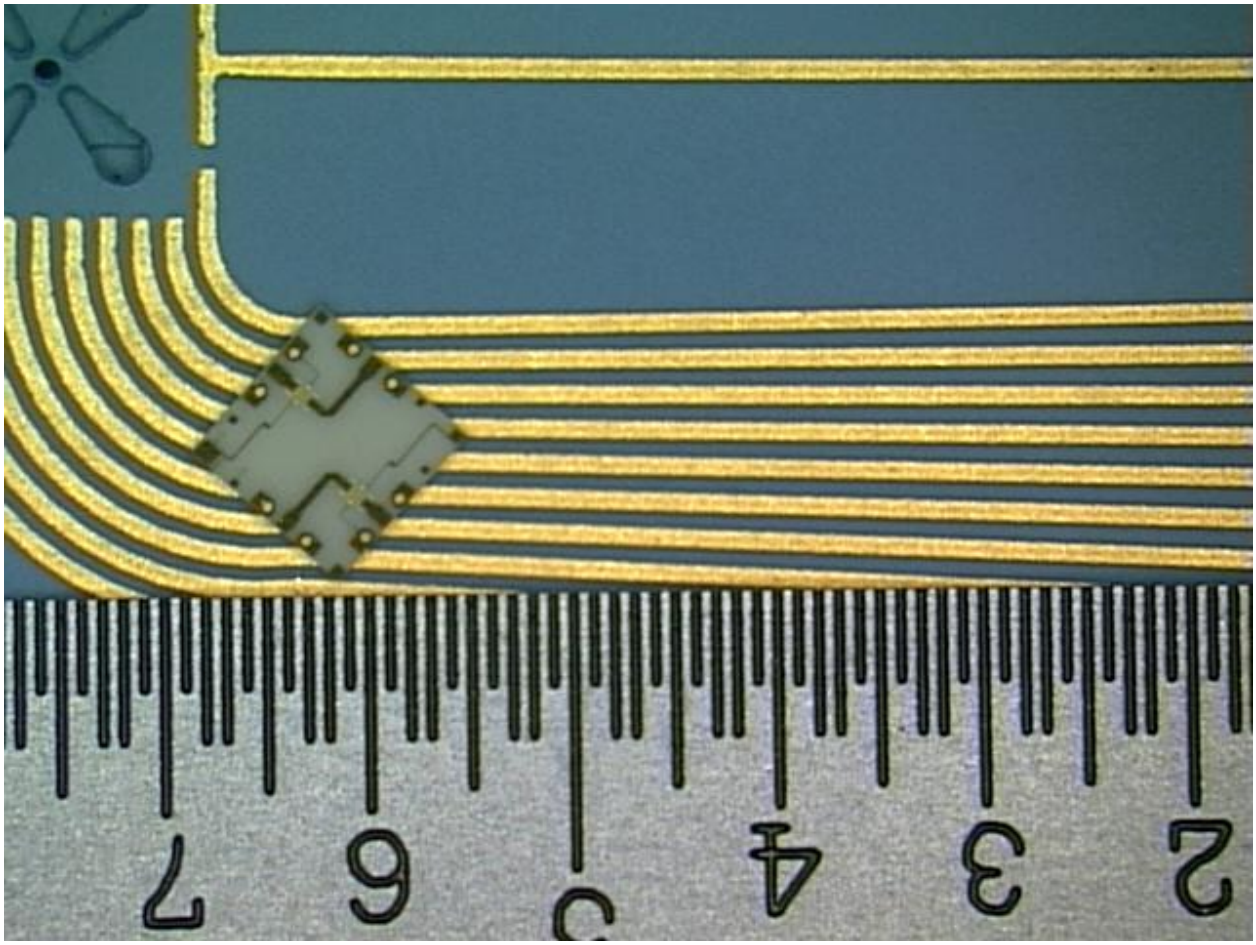

Figure 1. A Sandia Ohmic RF Switch MEMS part placed on the tip of a fluidic fixture from an unrelated MEMS project. The distance from the 6 to the 7 on the scale is 0.1 inches.

Static X-ray Imaging

Our first step in conducting a due diligence investigation was to acquire Sandia's first images of the switch part using laboratory X-ray machines. While the MEMS part was not in a package, the X-ray images taken perpendicular to the switch substrate record X-rays that pass through the 10 mil alumina substrate as well as through the few microns of gold that comprise the switch parts on top of this substrate.

We designed and fabricated a test fixture suitable for observing dynamic RF Ohmic Switch operation on laboratory X-ray machines, as shown in Figure 2. The fixture is an inexpensive FR4 circuit board that holds the MEMS switch near an X-ray source and connects the switch's high voltage control inputs to convenient BNC connectors. Additional BNC connectors provide for source and sense probes for 4-terminal measurement of contact resistance. We procured the circuit board from www.pcbexpress, with routing to shape by Circuit Shop Inc, Albuquerque.

Figure 3 is the placement and wire bonding diagram that Katherine Myers, 01715, followed to install a switch on one of our circuit board fixtures. In this position only the lower of the two switches on the part substrate is exercised and imaged. The measurement methodology described here demands only a single X-ray view taken perpendicular to the switch substrate. However, when making static measurements on a switch part, multiple X-ray views are easily obtained, and may be used for tomographic analysis. The position of the switch on our fixture may allow acquiring multiple views without interference from the plated-through holes in the bonding pads.

We acquired static X-ray images of an RF Ohmic Switch part using a micro-source X-ray machine operated by Sandia National Laboratory Organization 01522, and using a nanofocus X-ray machine operated by our organization 08722. Figure 4 shows the configuration of the nanofocus X-ray machine. The imaging detector is closest in photograph. The sample is on a robotic positioning mount, just behind the imaging detector. The X-ray source is behind the sample. This system is operated by Dan Morse, 08772, at Sandia's California site. The detector is from Photonic Science France, http://www.photonic-science.co.uk/PDF/XDI-VHR.pdf, and the source is from Feinfocus, http://www.comet.ch/security-inspection/feinfocus/open-micro-

nanofocus-x-ray-tubes/transmission-tubes/. The micro-focus X-ray machine is similar in configuration, is also from Feinfocus, and is operated by Kyle Thompson, 01522, at Sandia's Albuquerque site.

Figure 5 shows a micro-focus X-ray image of the switch part, taken perpendicular to the switch substrate. Figure 6 shows an image of the same switch part acquired using a light microscope. The top image in Figure 7 is a cropped close-up of the X-ray image displayed in Figure 5. The bottom image in Figure 7 is a second X-ray image acquired while the switch was oriented with the line between the X-ray source and the detector approximately parallel with the switch substrate.

Figure 8 shows an image of a second instance of the switch part acquired on the nanofocus X-ray machine. The X-rays for this 120 second exposure were 25 kV at 0.3 W. The source-to-camera distance was 10 cm and the source-to-object distance was much less than 10 cm. The bottom image in Figure 8 is a cropped and rotated version of the top image.

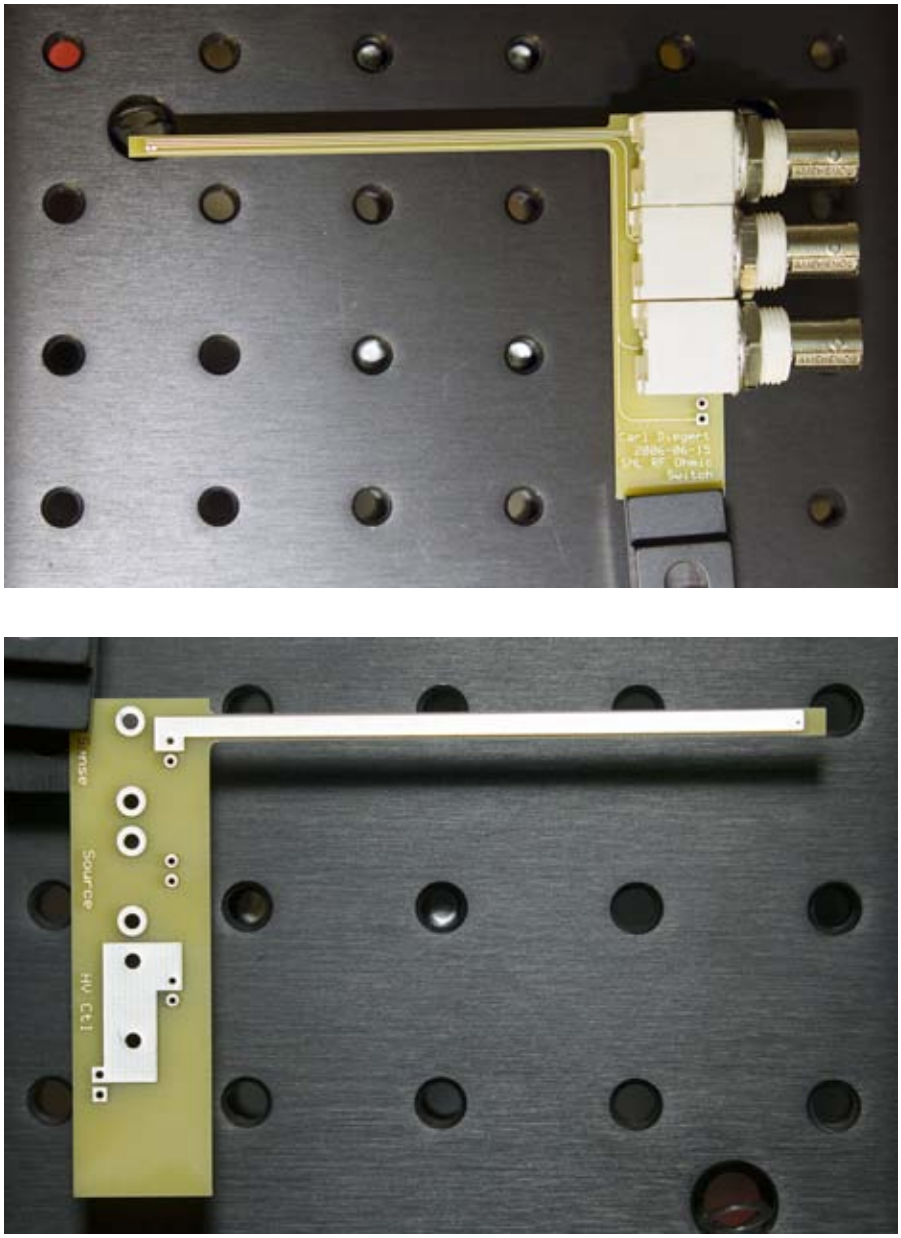

Figure 2. Circuit board fixture to operate switch during imaging on X-ray machine.

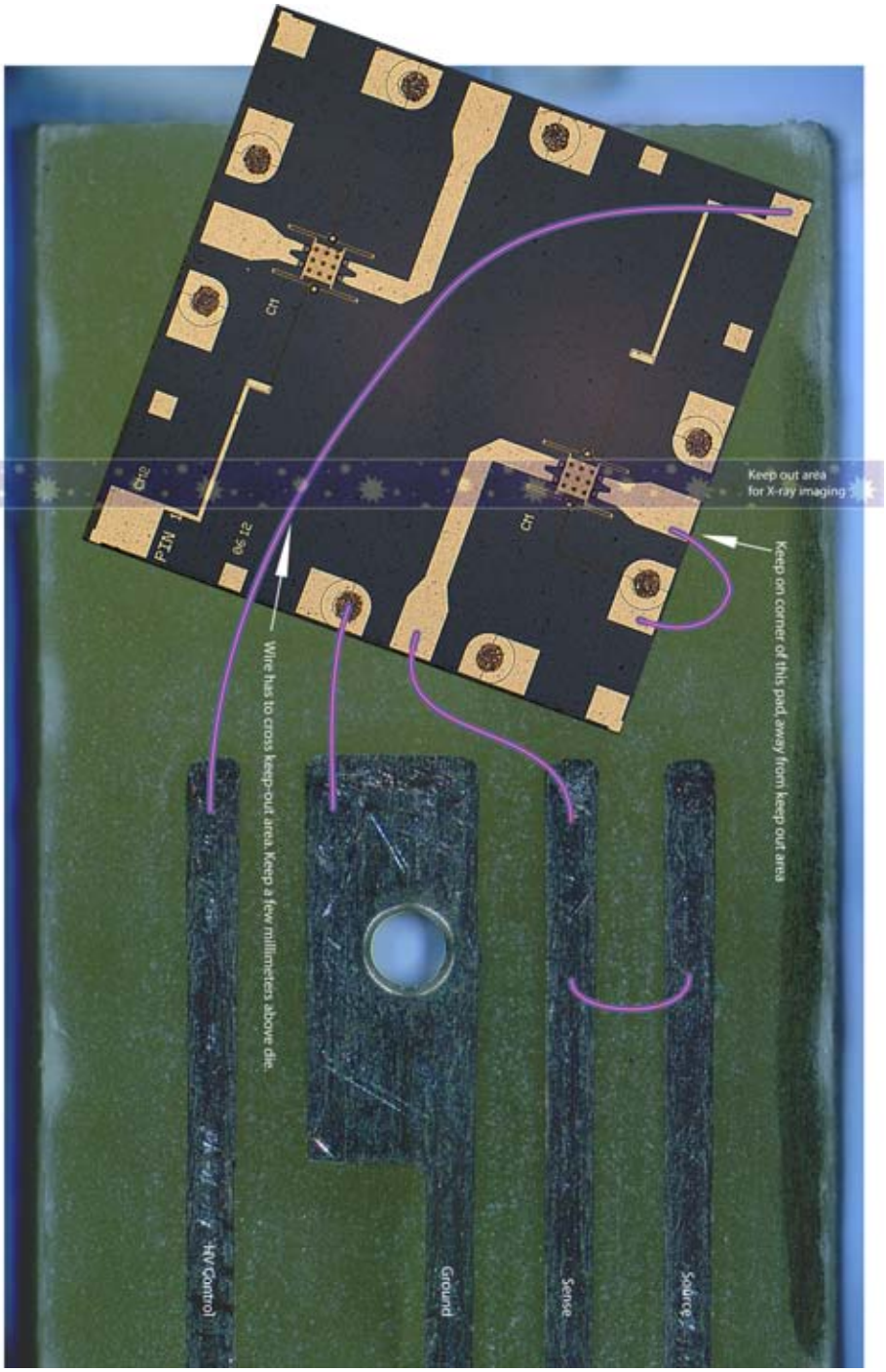

Figure 3. Placement and wire bonding for switch on tip of fixture.

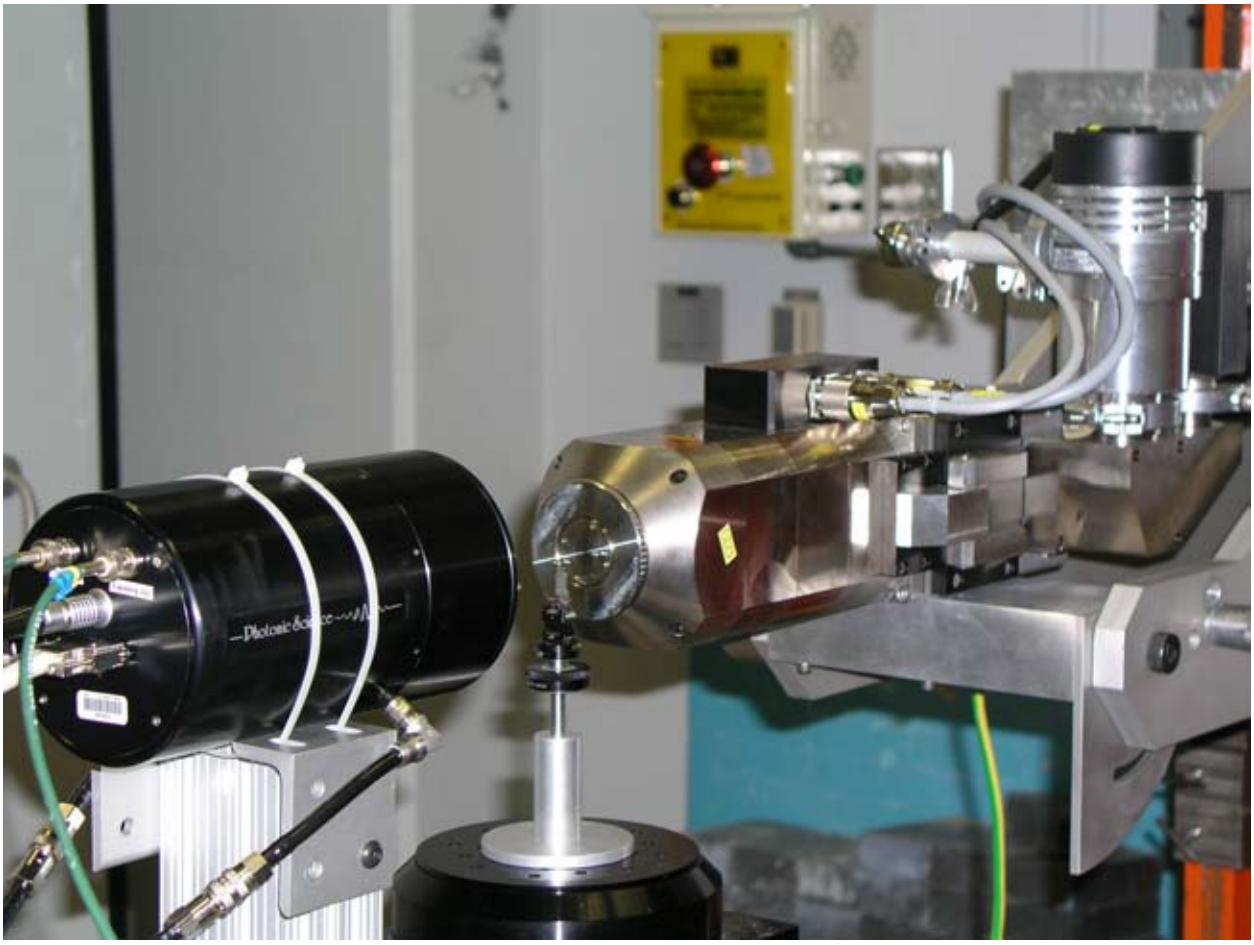

Figure 4. Configuratioin of nanofocus X-ray machine.

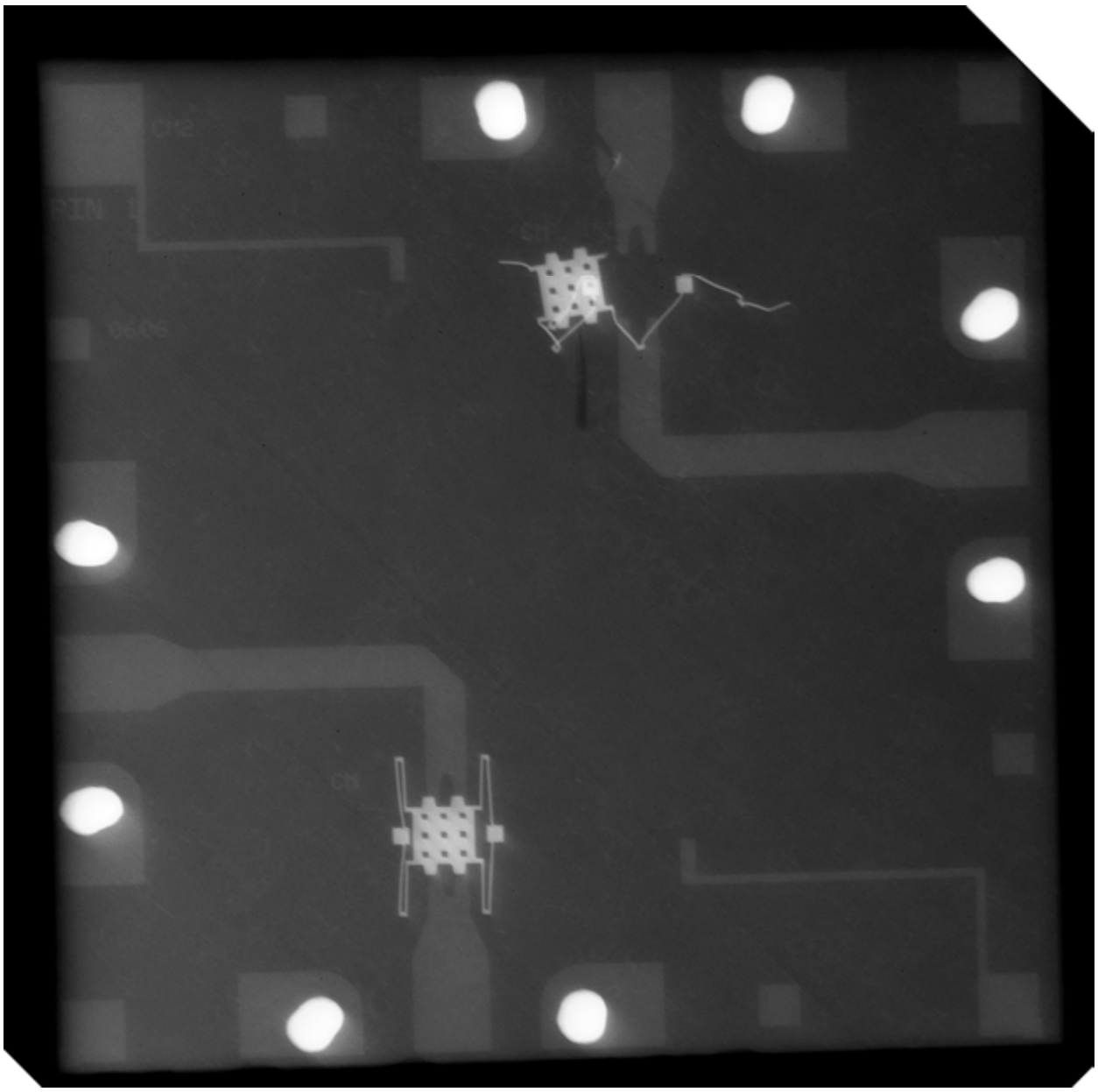

Figure 5. X-ray image from microfocus (about 6 micron spot size) Feinfocus machine.

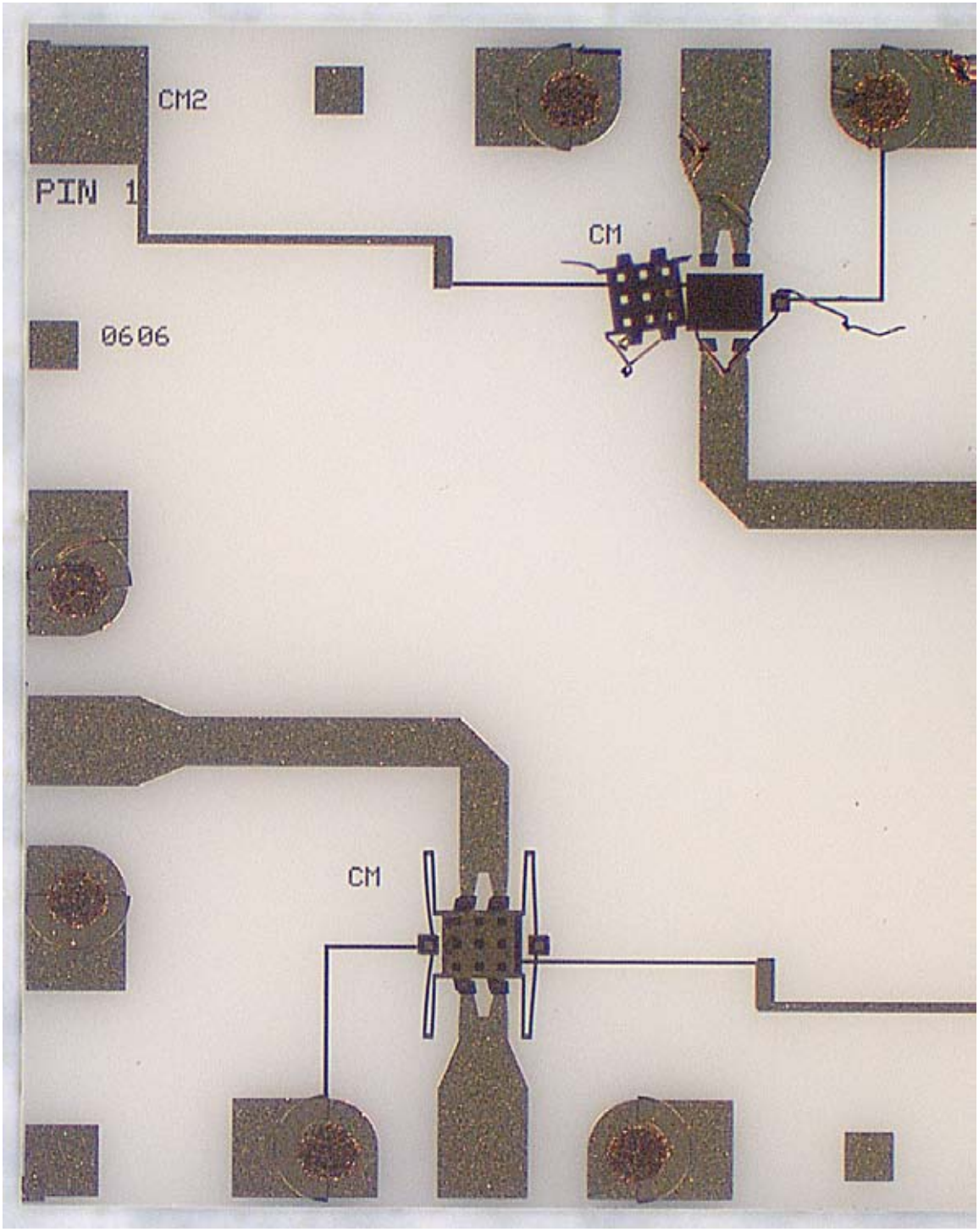

Figure 6. Light microscope image of the switch sample also shown in Figure 5.

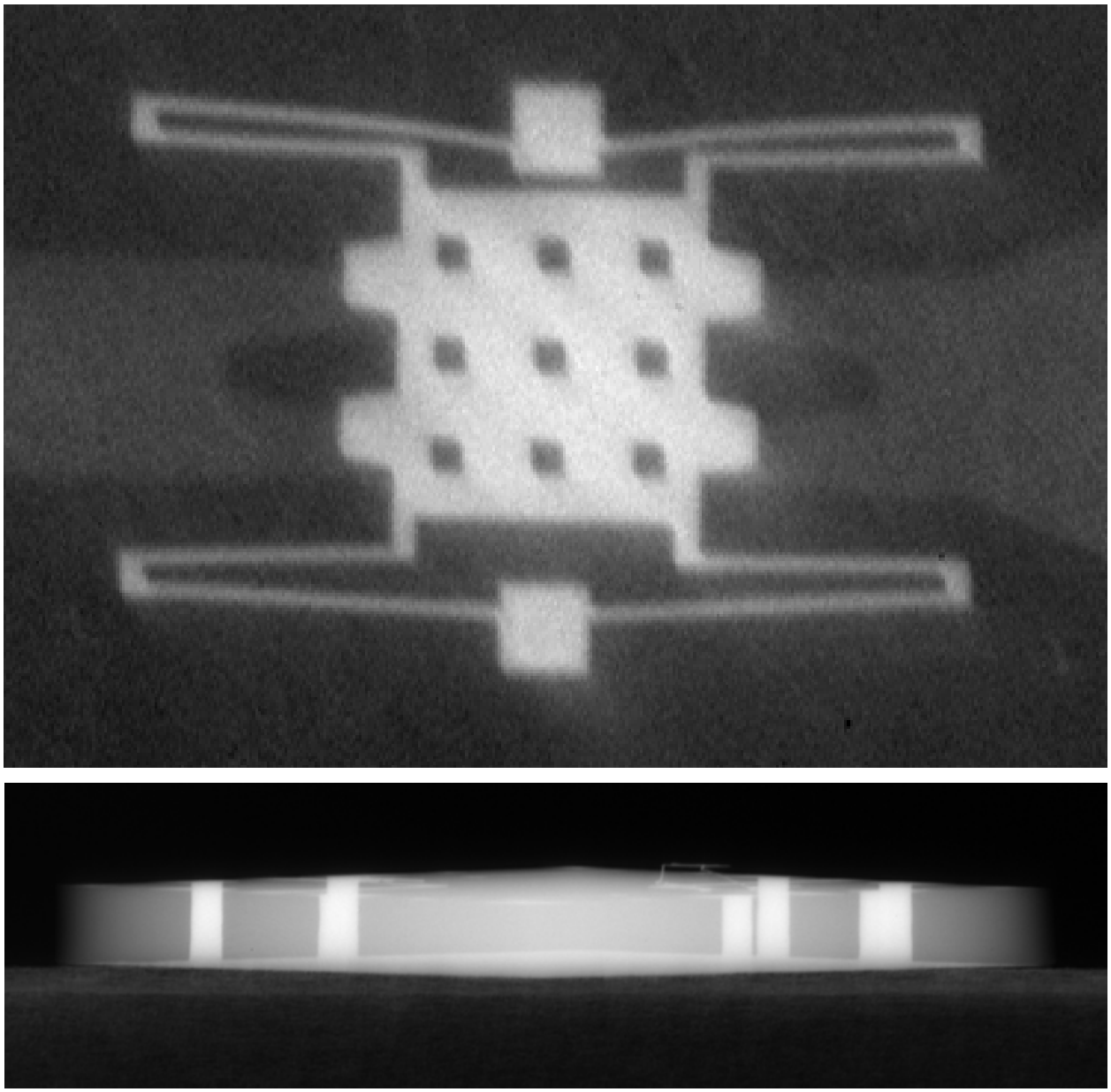

Figure 7. Top: A cropped, close-up of the X-ray image displayed in Figure 5. Bottom: A second X-ray image with film exposed while the switch was oriented with the line between the X-ray source and the detector approximately parallel with the switch substrate.

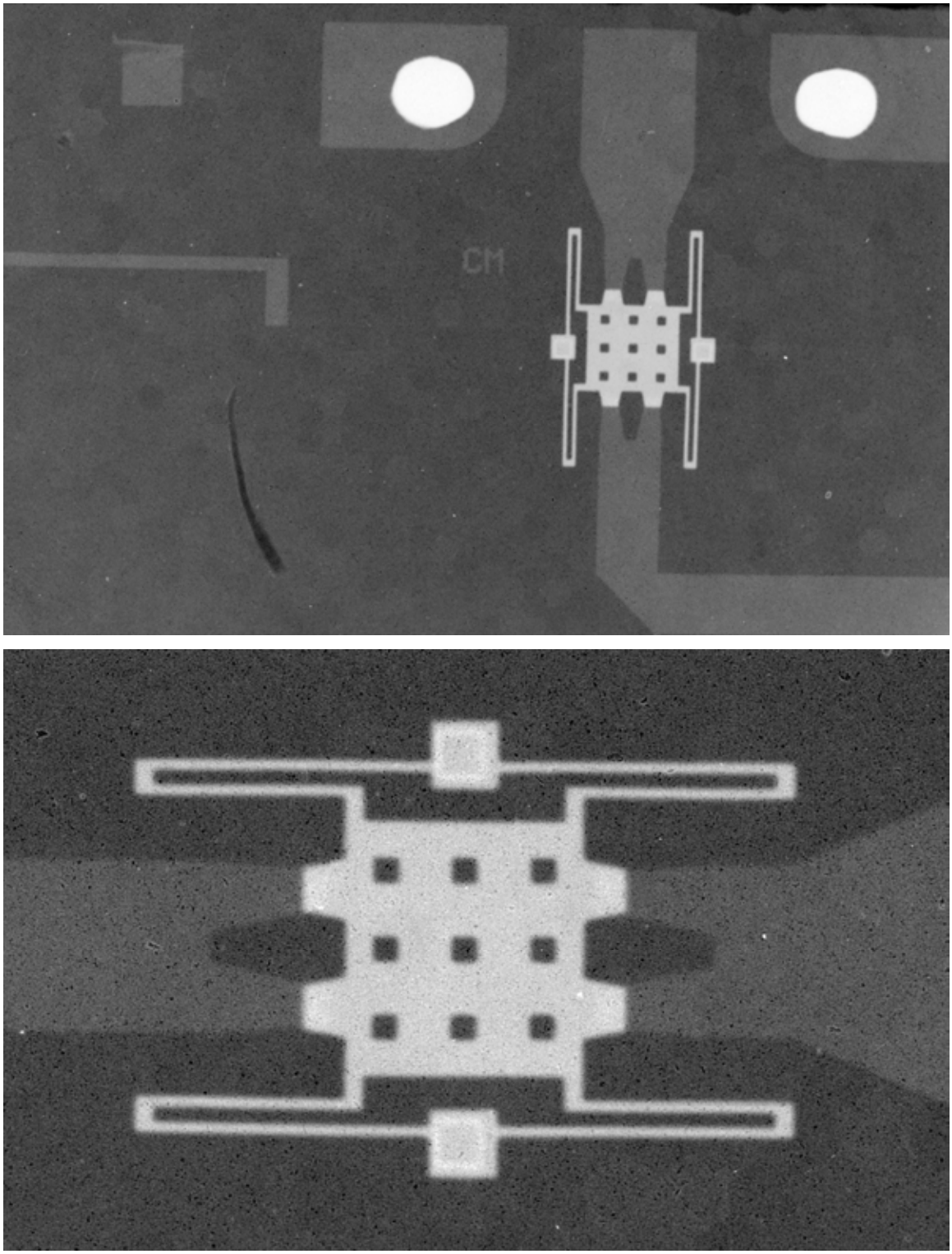

Figure 8. Another swich imaged using nanofocus X-ray machine.

Dynamic X-ray Imaging

It may be possible to acquire deformation of the crab at a specified instant of time by either pulsing the X-ray source, or shuttering the imaging detector. The range of important resonant frequencies in the Sandia Ohmic RF Switch crab extends up to tens of kilohertz. Therefore, a single exposure that freezes the high frequency motions of the switch will have to be a few microseconds or less. To acquire enough X-ray signal to overcome the statistical uncertainty of small counts of detected photons it will probably be necessary to operate the switch for many cycles, and accumulate images at a specified phase in this cycle (stroboscopic imaging).

Unfortunately, the nanofocus X-ray machine that captured the image in Figure 8 was unable to acquire useful static images during our brief due diligence investigation due to what turned out to be a failed lens power supply. The diagnosis and repair were completed in early December, 2006, and the image in Figure 8 acquired on 13-December-2006.

We have verified that the Feinfocus X-ray source in this nanofocus machine can be pulsed, with the control signal to the X-ray tube deflecting the electron beam inside the tube to turn the production of X-rays on and off. We have also verified that the Imaging Sciences imaging detector in this machine can be shuttered, with the control signal to the detector modulating its sensitivity to photons produced by the X-rays that penetrate the device under test. Unfortunately, we were not able to complete any stroboscopic X-ray imaging of switch parts during this brief project.

Ground-Truth Surface Topography

We acquired surface topography of an operating RF Ohmic Switch from an ultraviolet light confocal microscope operated by organization 05624. We completed careful, but conventional analysis on confocal image stack to show that the directly-observed topography showed that activating this particular switch part produces a 400 nanometer bend in its plate.

Figure 9 is an image computed from a collection of 51 images acquired by Peter Esherick, 05622, using a custom-configured, ultraviolet-light, confocal microscope from Tim Drummond, 05917. For each image in this stack, the microscope scanned the switch crab at an incremented height, where height is measured perpendicular to the switch substrate. Larger height values denote increasing height above the substrate, and the height is incremented by 400 nanometers between images. We pulled the RF Switch down to the switch on position before acquiring this image stack by applying and holding a control voltage of 80 volts. The extended depth of focus effect in this maximum-intensity projection, MIP, image is achieved by displaying, for each pixel position, the pixel value with maximum intensity among corresponding pixels at all 51 height values. The two vertical lines show the region we chose to analyze in Figures 14, 15 and 16 below.

Figure 10 is an image computed from the same image stack as for Figure 9, but with a computation that shows surface topography rather than a grayscale image of the surface color. For this computation, the height value at a pixel location is the height where maximum intensity of all the pixels in the stack occurs. Pixels are brighter when the top surface of the MEMS is higher above the switch substrate.

Figure 11 shows the same topography information as Figure 10, with a perspective rendering of the surface topography replacing the use of grayscale values to show height. Additionally, Figure 11 shows the grayscale *color* of each pixel as the *color* of the pixel from Figure 9.

Figure 12 is the result of filtering the information in Figure 11. The filtering suppresses some of the errors in estimating the surface by comparing the value of a pixel to the median of the nine

pixels in the three-by-three neighborhood adjacent to the pixel. When the difference was more than ten percent of the median value, the filter substitutes the median value for the pixel's value.

Figure 13 shows the switch in the same manner as Figure 12, but with the control voltage to the switch turned off. That is, the surface shown in Figure 13 was computed a different image stack acquired while the switch was in an off position.

Figure 14 shows how the switch crab moves in height as we cycled it on and off with voltages of 0, 70, and 80 volts. Each unit in the vertical scale is 400 nanometers, the center-to-center distance between our confocal image slices. This figure shows topography only along a *fat* vertical line from top to bottom of the switch as imaged in Figures 9 and 10. Line width extends from pixel column 371 to column 393 (33 columns wide), as shown by the two white vertical lines in Figures 8 and 9. For each of the five curves plotted in Figure 14, the mean of the 33 height values is plotted for each of the 1024 image rows.

Figure 15 shows the measurements from Figure 14, but with adjustment for a systematic error made by the confocal microscope stage used in their acquisition. The problem with the stage is that between acquiring image stacks, the absolute position of the height values can slip. To correct for this slip, we computed and subtracted the mean height in each acquisition between rows 30 and 80, positions where the switch part presents a gold conductor that is fixed to the alumina substrate and does not move.

Figure 16 shows the difference between the position of the switch crab in its down (on) and up (off) positions. That is, this figure shows how the shape changes when the activating voltage pulls the switch into the on position. These measurements show that the shape bows, as might be expected if the electrostatic force pulling all along the switch plate acts on a relatively soft gold plate between the contact posts supporting the plate at its ends. At the midpoint of this fat vertical line through the switch crab, the bowing brings the crab body about 400 nanometers (one unit on the vertical scale of this plot) closer to the fixed plate on the substrate than it would be if the crab moved as a rigid body.

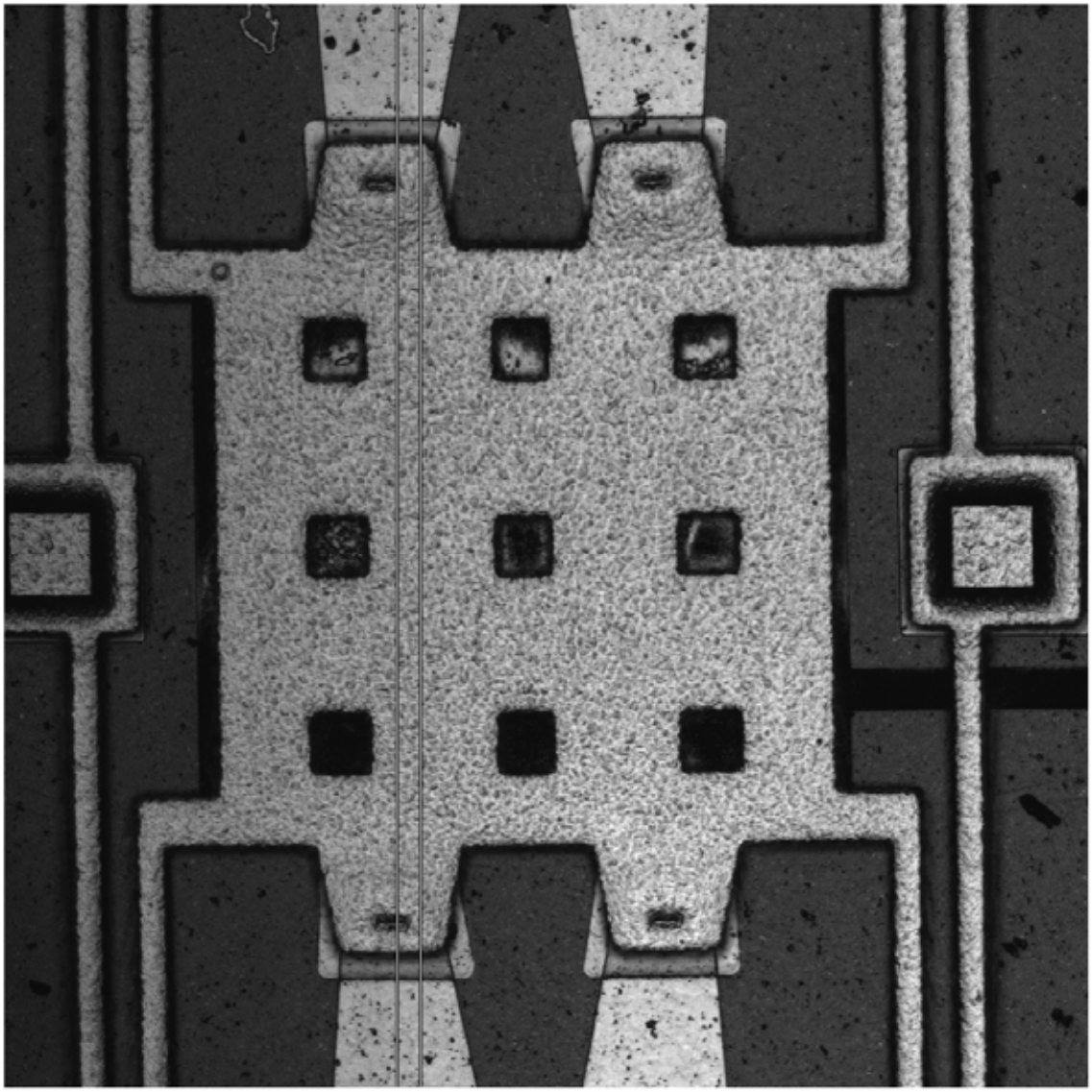

Figure 9. MIP image with switch crab pulled down.

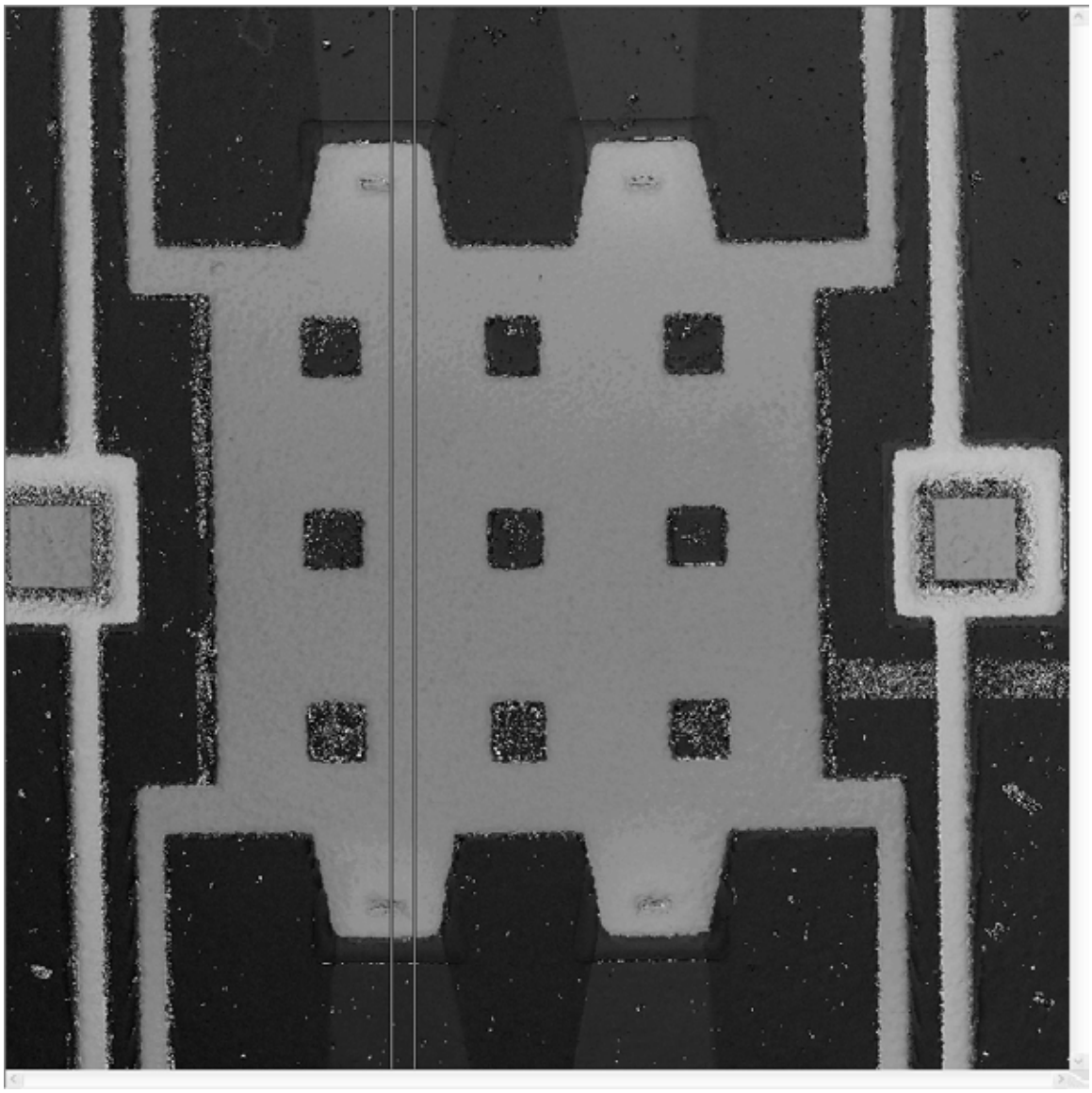

Figure 10. Surface topography with switch crab pulled down.

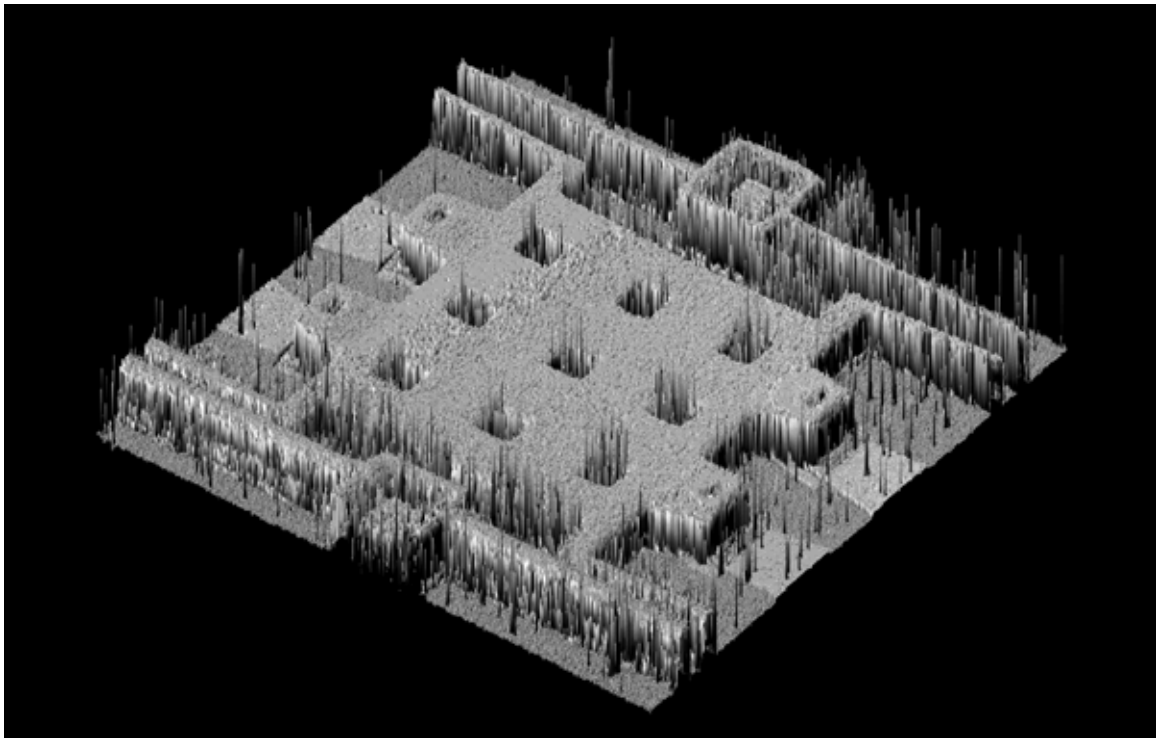

Figure 11.Combined topography and color information with switch crab pulled down.

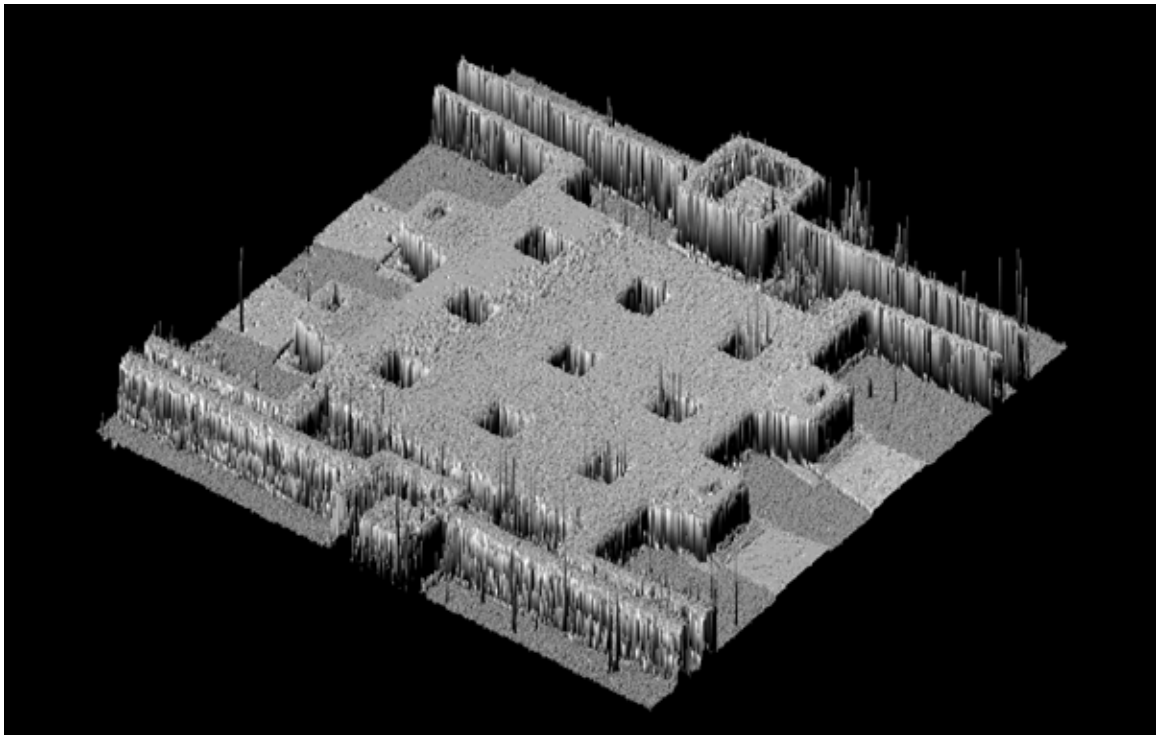

Figure 12. Filtered topography and color with switch crab pulled down.

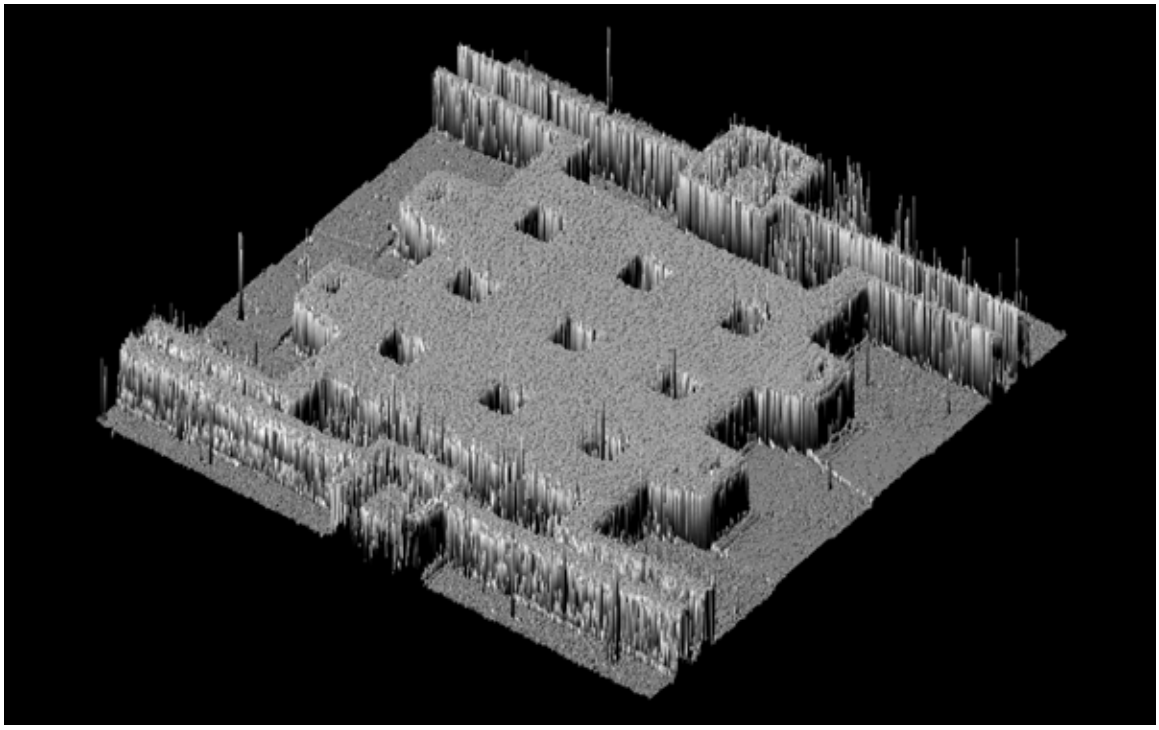

Figure 13. Filtered topography and color with switch crab released (off position).

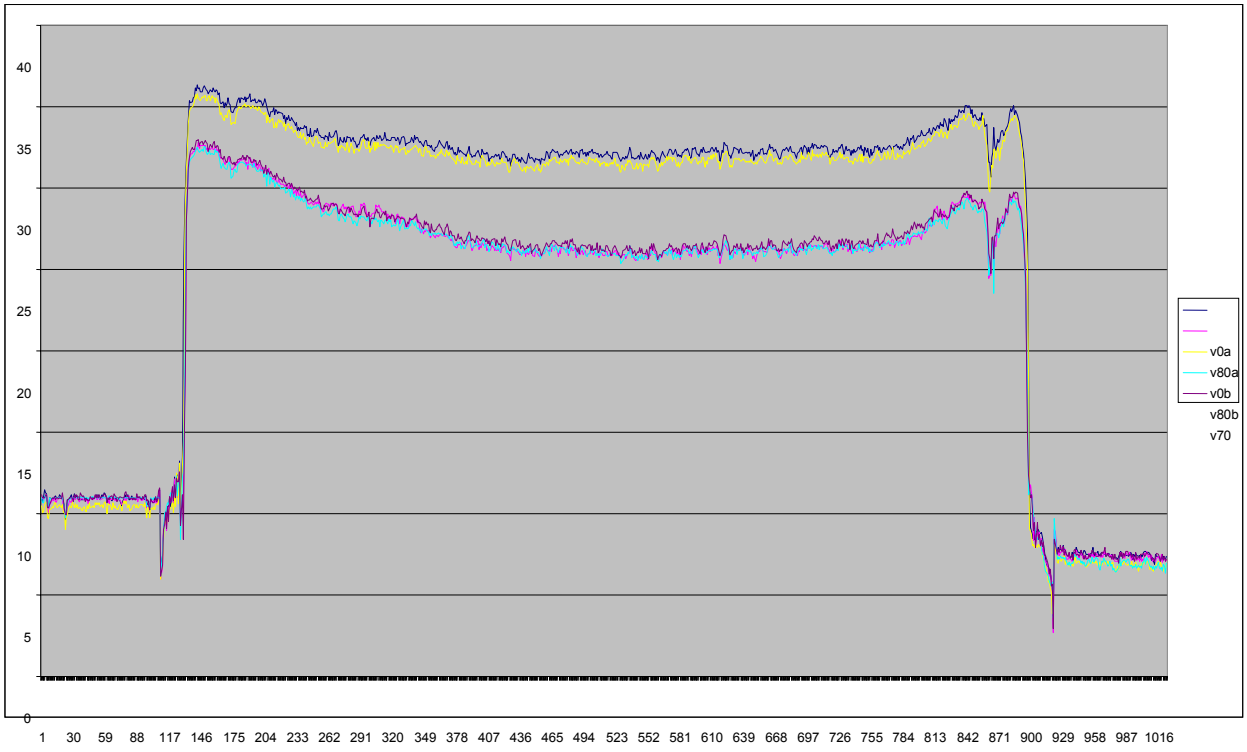

Figure 14. Switch crab height with control voltages of 0, 70, and 80.

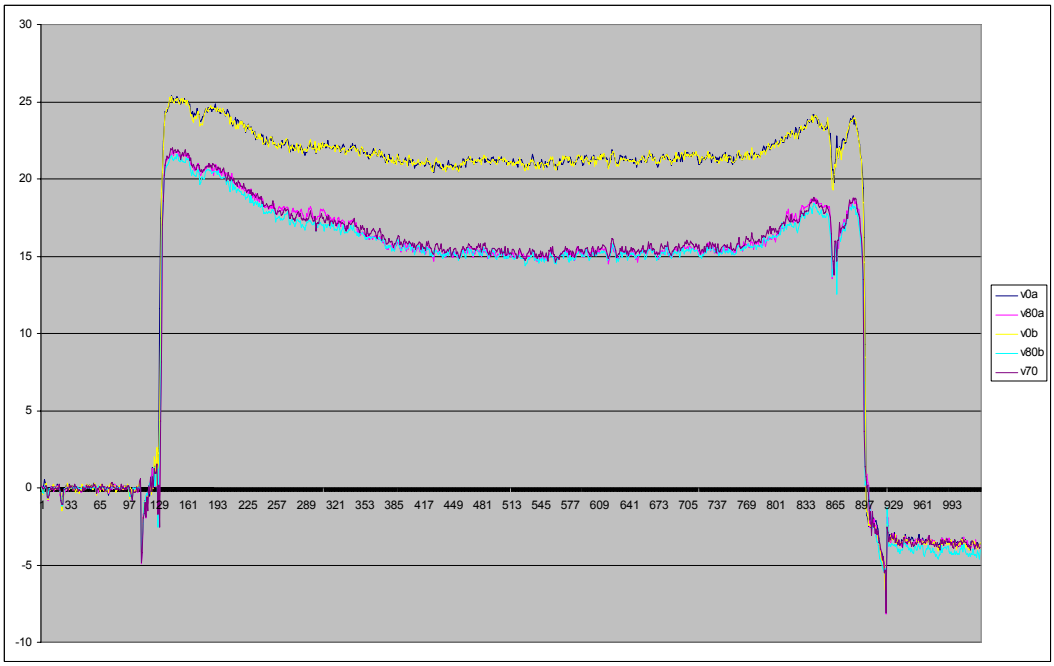

Figure 15. Switch crab height with control voltages of 0, 70, and 80 with correction for stage slip.

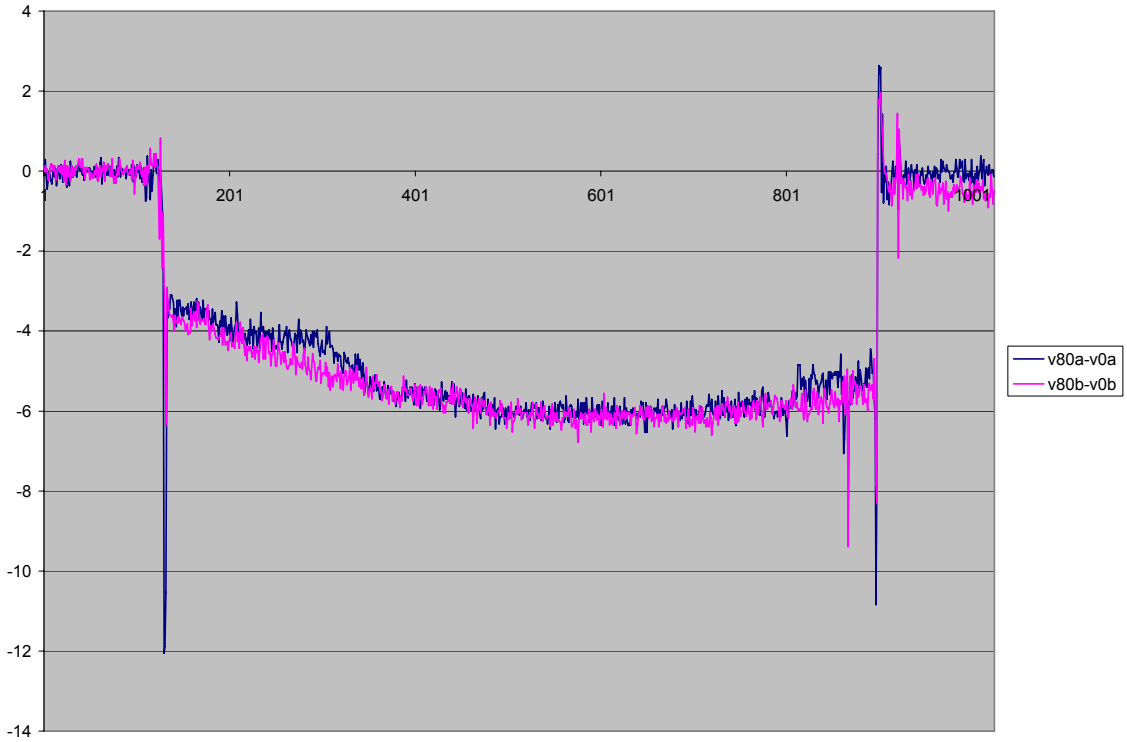

Figure 16. Difference between the position of the switch crab in its down (on) and up (off) positions. Bend is a departure from rigid body movement of about 400 nanometers.

Deformation from MIP light image

With X-ray images from above the switch substrate we record only the integral value of X-ray absorption as a ray passes vertically through the switch part. With these X-ray images we can observe in-plane movement of the switch crab, but cannot directly observe the out-of-plane, height component of the crab's surface topography. Recovering height information from maximum intensity pixel, MIP, images like Figure 9 is related to processing X-ray images. Like an X-ray image taken from above the switch substrate, the MIP images of the switch part in on and in off positions provide information on in-plane movement of the switch crab, but suppress the information on out-of-plane crab movement from the confocal image stack.

We performed a speckle correlation analysis of MIP images of the switch crab in on and off positions. This processing recovered sub-pixel, in-plane deformation (movement) of the plate with enough precision to indirectly imply an out-of-plane buckling deformation. The implied buckling is consistent with the surface topography directly observed with confocal imaging (Figure 16).

Figure 17 shows estimated in-plane deformation of the switch crab based only on a pair of MIP confocal images. Analysis of white light images of speckle patterns is a workhorse tool for Tim Miller, 01534 and Phillip Reu, 01526. They applied a commercial software package, Vic2D from Correlated Solutions, Columbia, South Carolina, to obtain these estimates from the image shown in Figure 9 and a corresponding image with the crab in the off position. The naturally-occurring patterns in the gold crab provided features for this correlation analysis.

The geometry of the switch crab helps interpret the Figure 17 result. The switch crab is about 150 microns high. A one-micron bowing at the center of a 150 micron high crab will, roughly, cause an in-plane movement of the top and bottom crab edges of

75 – sqrt(75^2 – 1) = 0.007 microns = 7 nanometers.

The pixels in the 1024-by-1024 confocal images are about 0.26 microns center-to-center. A one micron bowing, then, should produce an edge movement of 0.007/0.26 = 0.02 pixels. If the bowing was distributed over a shorter distance, then the edge movement would be larger.

The estimated deformation movement in Figure 17 is in pixel units. Note that the estimate shows both the crab's northwest and southeast corners moving toward the crab's central point. This in-plane movement is consistent with a crab that deforms by bending up at these two corners, defining a valley that runs from the crab's southwest to its northeast corners.

Deformation from X-ray image

Comments on future work with X-ray images are in the discussion section of this paper.

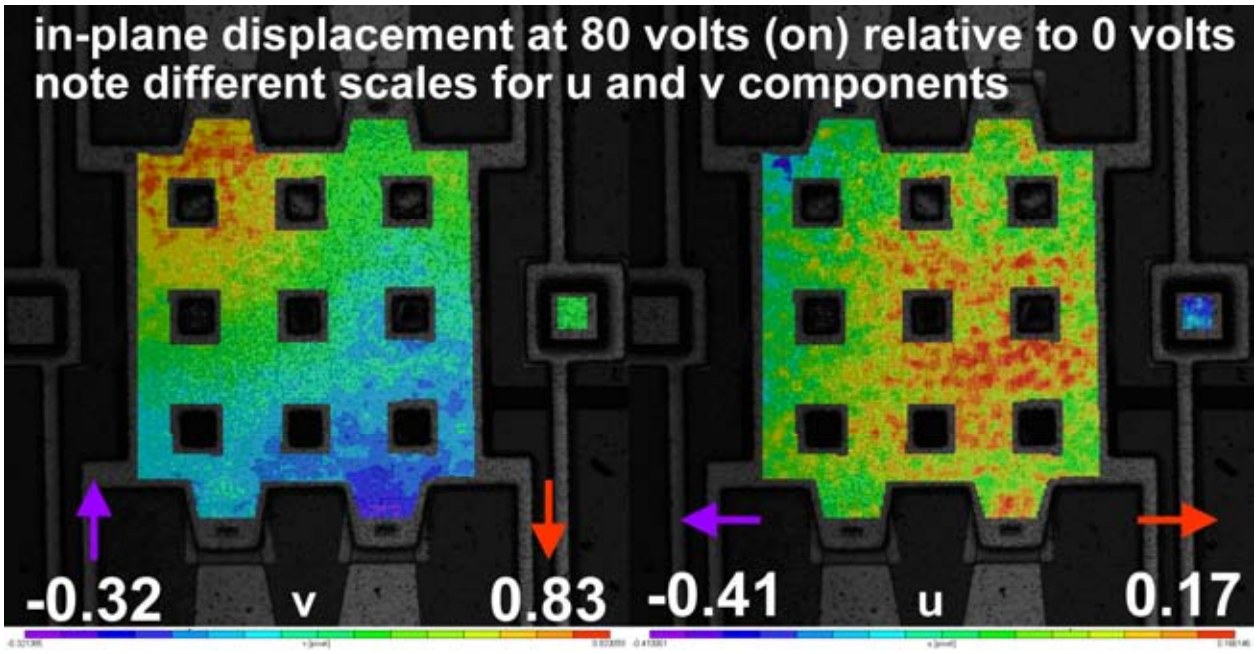

Figure 17. Estimated in-plane deformation computed from MIP confocal images.

DISCUSSION

Deformations of the crab component in the Sandia Ohmic RF MEMS Switch that depart from rigid-body movement by just one micron are important in the switch design. The current switch design largely constrains in-plane movement of the switch crab. It is deformation that departs from rigid-body movement by just one micron in the out-of-plane component that we want to detect. Our analysis using maximum-intensity-projection, MIP, summaries of confocal image stacks as a surrogate for X-ray images defines a methodology that may be able to observe these deformations without opening up the device under test for scanning with light. MEMS devices typically operate identically for many thousands of cycles. X-ray observation synchronized to operation of the device under test should be able to accumulate imaging at a defined phase of the cycle, estimating deformation at that instant in time.

Estimating out-of-plane deformation

Measuring a micron-scale, out-of-plane deformation of the 150 micron crab indirectly from the corresponding nanometer-scale, in-plane movement demands considerable statistical power. We believe that using computationally-intensive numerical simulations can enable engineers to define a modeling basis for new statistical methods, and that the new methods will improve on the statistical power of the analysis in Figure 17. It will be useful, and possibly essential to gain more statistical power to adequately complete analysis with X-ray imaging used in place of the surrogate MIP light images.

It may already seem remarkable that the correlation analysis behind Figure 17 can estimate a deformation of only 1/100 of a pixel. However, the Photomechanics literature reports that this precision is routine for analysis of white light images of speckle patterns without resorting to interferometric or diffraction methods [1, 2]. What this literature calls Digital Image Correlation technique, DIC, was originally developed to measure homogeneous deformations on the surfaces in order to resolve very small strains. In DIC a subset-based correlation algorithm is employed to

mathematically match subsets of intensity data from an initially undeformed image with subsets of intensity data from a deformed image that are reconstructed with subpixel accuracy using interpolation schemes.

The particular assumptions that define the subsets of the DIC technique constitute a mathematical model. This model then defines how image pixel values are combined to form deformation estimates. Statistical power is gained when the many degrees of freedom in the image pixel data are reduced to a relatively few degrees of freedom that define the estimated deformation. For example, if each pixel is observed with an error that is uncorrelated with the errors in other pixels, then a *Central Limit Theorem* argument shows that taking the mean of a subset of pixels reduces the error by the square root of the number of pixels combined. The Photomechanics literature reports on more complex statistical models for errors in pixel values, and on more complex functions that combine pixels into deformation estimates.

A mathematical model defined to specify all possible deformations of the switch crab can have far fewer degrees of freedom than the general subset-based model underlying the DIC technique. For example, a list of parameters to define a list of vibration modes that are superimposed to define crab deformation is much shorter than the list of parameter values to define a large grid of displacement vectors that are interpolated to define deformation. The additional reduction in degrees of freedom is likely to be a basis for increased statistical power, as explained in the *Materials and Methods* section of this report. Numerical experiments with high-fidelity, finite-element models of the switch crab are likely to be a basis for creating a suitable model.

Moving to nanofocus X-ray imaging

Examining the recent nanofocus X-ray image of the switch crab in Figure 8 suggests some next steps toward realizing the new methodology for measuring crab deformation. The comments here are preliminary, as this first nanofocus image was acquired on 13-December-2006.

To estimate crab deformation, the challenge is to statistically process images like Figure 8 to find features in the gold switch crab and to reject features in the alumina substrate. Simple next steps,

demanding just additional time on the X-ray machine, are to get some more magnification by moving the switch crab closer to the X-ray source, and to adjust exposure time to acquire larger pixel counts for pixels in the switch crab.

For statistical processing for nanofocus X-ray imaging, we would use correlation of the alumina features to register two X-ray images with precision of less than 1/100 of a pixel. Next we would *subtract out* the Alumina features based on the fact that these features do not move from one image to the next. Success will demand careful attention to interpolation details, and not just simple subtraction. The result should be features that do move, hopefully features from the gold switch crab that we deliberately moved from the switch "on" to the "off" position. The model-based estimation described in this report, then, can compute deformation estimates from these features.

Examining Figure 8 shows another problem with trying to estimate crab deformation from only accurate estimation of its edges. The problem already described in this report is that there are few pixels contributing to estimates of edge location relative to the number of pixels that can contribute to model-based deformations of the whole crab surface. The new problem is that the X-ray image appears to resolve the crab edges much more poorly than the smallest features in the substrate and the crab materials. Scattering of X-rays at the edges could be the physical cause of this disparity. Whatever the cause, it is another argument for modeling the whole of the crab, and basing deformation estimates on all the pixels that image the crab.

Impact

With human ability to understand simulation results, computationally-intensive numerical solution can be used as an integral part of making difficult, nanometer-scale measurements. This innovation breaks the constraints implied when physical measurements are cast in a formal verification and validation (V&V) role. For V&V, measurements are made independently, without incorporating high-performance solutions to FEA or other computationally-intensive models. This report defines a role for solving a large FEA problem as an integral part of making measurements. The innovation is that the predictive capability of the FEA solution is assumed

correct, and forms a basis for measuring which dynamic deformations occur in the physical devices under test. The specific methodology can likely contribute important measurements on a variety of operating MEMS, making measurements that contribute to understanding dynamic operation of new thermal MEMS actuators that are complimentary to measurements made using interferometry (by Wyco and other instruments), and by laser doppler (by Polytech instruments). More generally, the work opens up a broad front of possibility where the ability of massive high-performance computers enables new measurements.

REFERENCES

1. Asunda, A. K., **MATLAB for Photomechanics A Primer**, Elsevier, Oxford, 2002.

2. Rastogi, P. K. (Ed.), **Photomechanics**, Springer, Berlin, 1999.

DISTRIBUTION

1	MS1318	David Womble	01410
1	MS1318	Scott Mitchell	01411
1	MS0370	Timothy Trucano	01411
1	MS1316	Carl Diegert	01412
1	MS1316	Mark Daniel Rintoul	01412
1	MS1320	Louis Romero	01414
1	MS0316	Scott Hutchinson	01437
1	MS0826	Chungnin C. Wong	01513
1	MS0555	Kyle Thompson	01522
1	MS1070	Hartono Sumali	01526
1	MS1070	Phillip Reu	01526
1	MS1070	Jordan Massad	01526
1	MS1139	Timothy Miller	01534
1	MS1076	Katherine Myers	01715
1	MS0892	Thor Osborn	01716
1	MS1424	Peter Esherick	01724
1	MS1076	Victor Yarberry	01737
1	MS1085	Christopher Dyck	01742
1	MS1069	Jonathan Wittwer	01749
1	MS1069	Michael Baker	01749
1	MS0959	Kenneth Peterson	02452
1	MS0822	Constantine Pavlakos	04326
1	MS1202	Warren Mial	05624
1	MS1202	Timothy Drummond	05917
1	MS1202	Timothy Berg	05624
1	MS9403	Daniel Morse	08772
2	MS9018	Central Technical Files	8944
2	MS0899	Technical Library	4536